Dipole-Mediated Interfacial Solvation for Efficient Li-Ion Transport in Dendrite-Free Li Metal Batteries

*Wenlong Zhao [a,b,‡], Kui Xu [c,‡], Yanyan Zhang *[a], Qingyu Dong [b], Ningyuan Zhang [b], Huihui Wang [b], Ruowei Yi *[b,d], Yuxin Tang [a], Yanbin Shen *[b], Liwei Chen [e]*

a College of Chemical Engineering, Fuzhou University, Fuzhou 350002, China

b i-Lab, Suzhou Institute of Nano-Tech and Nano-Bionics, Chinese Academy of Sciences, Suzhou 215123, China

c School of Flexible Electronics (Future Technologies), Institute of Advanced Materials, Nanjing Tech University, Nanjing, 211816, China

d School of Chemistry, Xiangtan University, Xiangtan 411105, China

e In Situ Center for Physical Sciences, School of Chemistry and Chemical Engineering, Shanghai Jiaotong University, Shanghai 200240, China

‡ Both authors contributed equally to this work.

*Corresponding author.

E-mail address: rwyi@xtu.edu.cn (Ruowei Yi), zyanyan@fzu.edu.cn (Yanyan Zhang), ybshen2017@sinano.ac.cn (Yanbin Shen)

Preparation of PP@LATSP and PP@Al_2O_3 Separators. Coating slurries were prepared by dissolving 4 g of polyvinylidene fluoride (PVDF, Aladdin) in 76 g of N-methyl-2-pyrrolidone (NMP, 98%, Aladdin) solvent, and then dispersing 20 g of LATSP particles (prepared by solid phase sintering) into the solution by vigorous stirring. Then, the coating was uniformly dispersed on PP separators (20 μm, Shanghai Enjie New Material Technology Co., Ltd., ND12), which were subsequently transferred to an oven to remove the solvent at 80°C. After 12 h, the single-side coated separator (PP@LATSP) was obtained. PP@Al_2O_3 separator was prepared using the same approach.

Preparation of PP@LATSP@DNA and PP@Al_2O_3@DNA Separators. DNA was grafted onto the PP@LATSP separator to fabricate the self-assembled layers. DNA was dissolved in methanol at a concentration of 10 g L^{-1}. Then the PP@LATSP separator was immersed in the prepared solution at 30℃ for 24 h. Afterward, excessive molecules on the LATSP were washed with methanol and ethanol 3 times in total. Finally, the as-prepared PP@LATSP@DNA separators were dried at 60℃ overnight. PP@Al_2O_3@DNA separator was prepared using the same approach.

Cell assembly and electrochemical measurements. All electrochemical measurements were carried out in a 2025-type coin cell configuration except for the pouch cell test. 60 μL electrolyte (1 M LiTFSI in DOL/DME with 2 wt.% $LiNO_3$) was added to each coin cell. For the Li||NCM811 cell, a 2M lithium bis(fluorosulfonyl)imide (LiFSI) in 1,2-dimethoxypropane (DMP) electrolyte was used as a substitute. The LFP and NMC811 electrodes in the lab were prepared by mixing LFP, super P, and PVDF dissolved in N-methyl-2-pyrrolidone (NMP) (the mass ratio of active materials: 96.5%). The slurry was then cast onto Al foil and dried at 100°C under vacuum for 12 h. The mass loading of LFP cathodes was 7.5 mg cm^{-2} or 16 mg cm^{-2}, according to the specific description. The

mass loading of NMC811 cathodes was 6.0 mg cm^{-2} or 20 mg cm^{-2}, according to the specific description. The Li discs with 450 μm thickness and 15.6 mm diameter were used as anodes in coin cells. For all the electrochemical tests, the PP@LATSP@DNA separator was used for validation, and the PP@LATSP separator as a control.

The Li||Li, SS||SS symmetric cells, Li||Cu cells, Li||LFP, and Li||NCM811 cells were assembled in 2025 type coin cells with 60 μL electrolyte. The VMP300 electrochemical workstation (Bio-Logic, France) was used to conduct the electrochemical impedance spectroscopy (EIS, frequency range: 7 MHz to 0.1 Hz, amplitude: 10 mV), chronoamperometry (CA, step potential: 10 mV, record time: 2 hours), cyclic voltammetry (CV, scanning speed: 0.1 mV s^{-1}) and linear scanning voltammetry (LSV, scanning speed: 0.1 mV s^{-1}). The galvanostatic cycling of coin cells was conducted using the system from NEWARE Battery Test System (CT-4008Tn-5V-10mA-164, Shenzhen, China). The single-layer pouch cell (0.17 Ah) is assembled in a dry room with a dew point temperature below - 50°C. The NCM811 cathodes (20 mg cm^{-2}, 6.25 cm×3.45 cm), thinner Li anodes (200 μm), and separators are assembled using the lamination method. The manufacturing process includes ultrasonic welding, packaging, and vacuum sealing with electrolyte injection.

Materials characterization. The scanning electron microscope (SEM) characterizations of Li anode morphology were performed using Hitachi Regulus 8230 at 5 kV. All samples were collected from coin cells disassembled in an Ar-filled glove box and rinsed with DME to remove residual electrolytes. The samples were transferred to the SEM chamber via a homebuilt gastight transfer device to protect the sample from ambient air.

X-ray photoelectron spectroscopy (XPS) characterizations of electrodes were all conducted on a PHI-5000 Versa Probe instrument employing Al Kα radiation. The samples were transferred from an Ar-filled glovebox by the custom-made transfer chamber with gastight sealing to the measurement chamber. The XPS depth profiles were obtained by Ar sputtering to remove the material layer-by-layer and then characterized. Time-of-flight secondary-ion mass spectrometry (TOF-SIMS) measurements were examined via TOF-SIMS5 (ION-TOF-GmbH) in a Vacuum Interconnected Nanotech Workstation (Nano-X).

Calculations Methods. Density functional theory (DFT) calculations of different solvents and lithium salts were conducted using a DMol3 module of Materials Studio software Geometric optimization and LUMO/HOMO energy calculations were performed by the generalized-gradient approximation Perdew-Burke-Ernzerhof (GGA/PBE) functional and double numeric polarization (DNP) basis set。

The induced dipoles of DOL, DME, and DNA molecules were calculated from the DMol3 module of the Materials Studio. Each molecule with one Li^+ was first subjected to the geometry optimization process using the GGA BLYP functional with a basis set of TNP 3.5. The convergence thresholds were set to an energy of $1*10^{-5}$ Hartree (Ha), a maximum force of $2*10^{-3}$ Ha $Å^{-1}$, and a maximum displacement of $5*10^{-3}$ Å. Then the induced dipoles of each molecule were obtained using the electrostatic moments analysis with the Fine grid resolution after the removal of Li^+.

The adsorption energies of a lithium-ion on the (113) crystal plane of LATSP and at two distinct sites after carboxylation were calculated using the Vienna Ab-initio Simulation Package (VASP), which is based on Density Functional Theory (DFT). A two-step computational strategy was employed. First, structural optimizations were performed using the Perdew-Burke-Ernzerhof

(PBE) generalized gradient approximation (GGA) functional. The DFT-D3 method was incorporated to account for dispersion forces, ensuring an accurate description of weak intermolecular interactions. A plane-wave cutoff energy was set to 520 eV. The convergence criterion for the electronic self-consistency loop was set to 10^{-5} eV, and all atomic positions were relaxed until the residual forces on each atom were less than 0.02 eV/Å. The conjugate gradient algorithm was utilized for ionic relaxation, with the cell volume held constant to eliminate any potential influence of substrate deformation on the adsorption configuration. A maximum of 2000 ionic steps were set to ensure that complex systems could fully relax to their minimum energy conformation. The electronic structure calculations were carried out using Gaussian smearing and real-space projection operators, which are well-suited for accurately describing the electronic properties of the semiconductor-molecule interface system investigated in this study. Following the structural optimization, a static self-consistent field (SCF) calculation was performed on the optimized geometry to obtain a more accurate total energy and charge density for the adsorption energy analysis. For this step, the electronic convergence criterion was tightened to 10^{-6} eV, and ionic relaxation was turned off. The adsorption energy (E_{ads}) for each configuration was calculated using the following formula:

$$E_{ads} = E_{total} - E_{surface} + E_{Li}$$

where E_{total} is the total energy of the slab with the adsorbed lithium-ion, $E_{surface}$ is the energy of the pristine LATP slab, and E_{Li} is the energy of an isolated lithium-ion in the same cell.

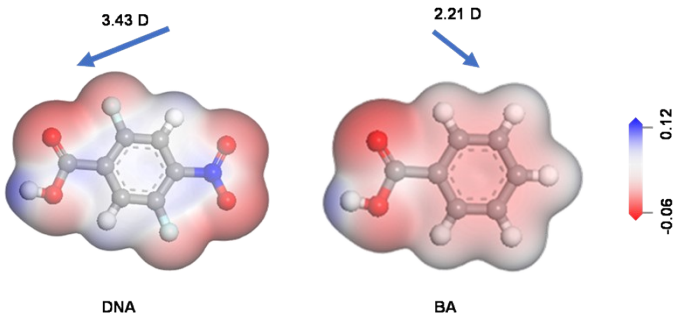

Figure S1. Calculated dipole moment and the orientations for different molecules.

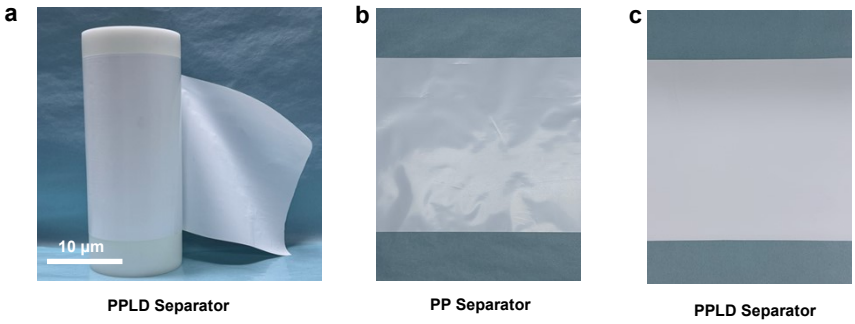

Figure S2. (a) Digital images of the PPLD separator prepared by roll-to-roll production processes. Digital images showing the surface of (b) PP separator and (c) PPLD separator.

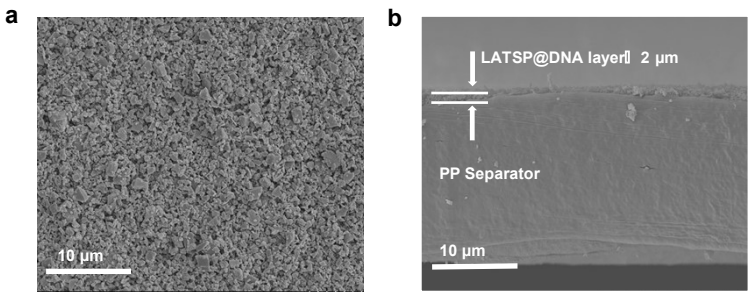

Figure S3. (a) Top-view and (b) cross-sectional SEM images of the PPLD separator.

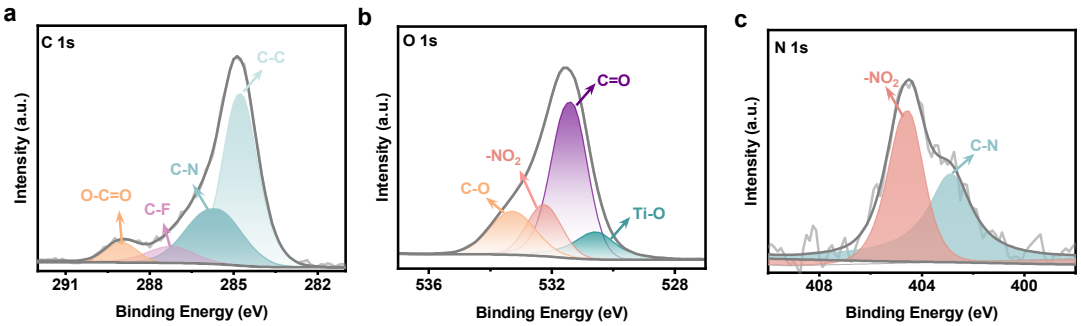

Figure S4. Detailed XPS fitting profiles of (a) C 1s, (b) O 1s, and (c) N 1s spectra of the PPLD separator.

Table S1. Ionic conductivity, $t_{Li+,}$ and Li^+ conductivities of different separators corresponding to Figure 1f.

	PP	PPA	PPAD	PPL	PPLD	PPLB
Conductivity at 30℃ (mS cm^{-1})	0.308	0.243	0.411	0.359	0.517	0.227
t_{Li+}	0.371	0.389	0.494	0.415	0.646	0.297
Li^+ conductivity (mS cm^{-1})	0.114	0.095	0.203	0.149	0.334	0.067

Table S2. Ionic conductivities of different separators at 30-70°C corresponding to Figure 1g.

Temperature (℃)	Ionic conductivities (mS cm^{-1})	
	PPL	PPLD
30	0.359	0.517
40	0.378	0.588
50	0.448	0.675
60	0.537	0.746
70	0.599	0.792

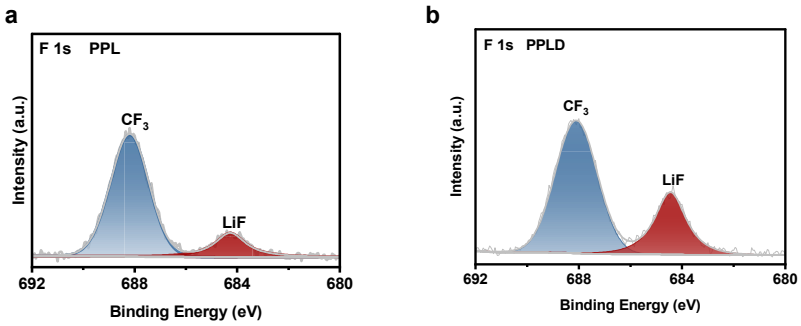

Figure S5. Detailed XPS spectra F 1s of the Li surface after 7-day rest in a Li||Li symmetric cell with (a) PPL separator and (b) PPLD separator.

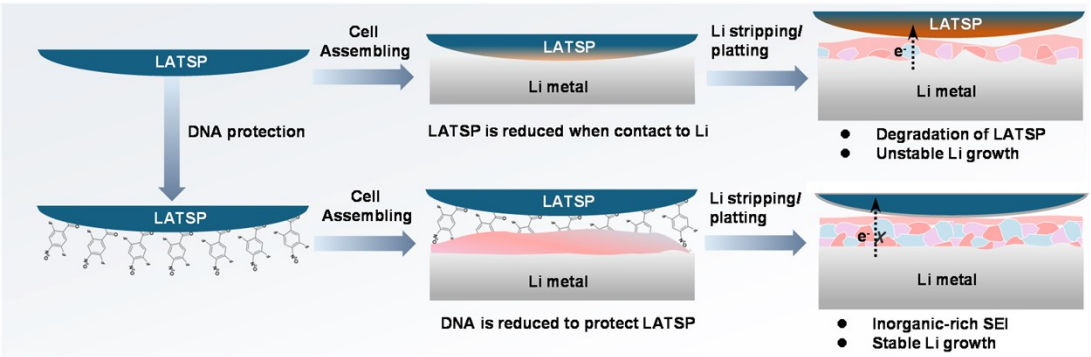

Figure S6. Schematic of the prior reduction of DNA and its contribution to the chemical and electrochemical stability.

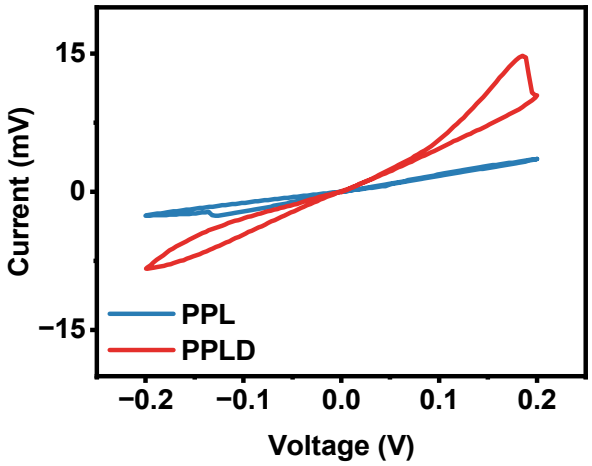

Figure S7. CV curves of symmetrical Li||Li cells with PPL and PPLD separators, respectively.

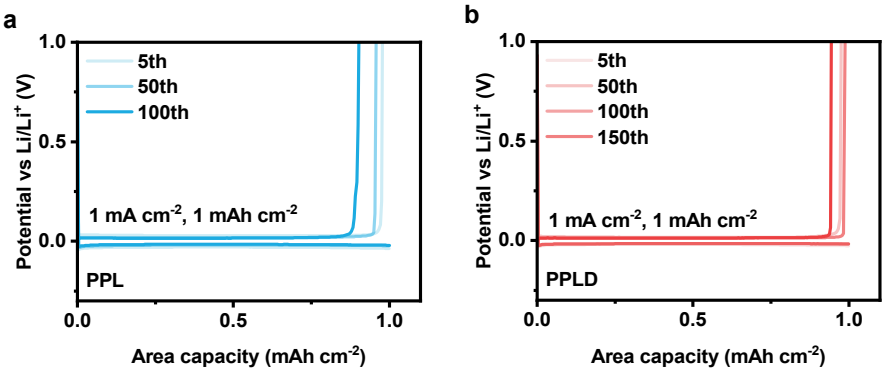

Figure S8. The deposition-stripping curves for different cycles in Li||Cu half-cells with (a) PPL and (b) PPLD separators at a current density of 1.0 mA cm^{-2} and a capacity of 1.0 mAh cm^{-2}.

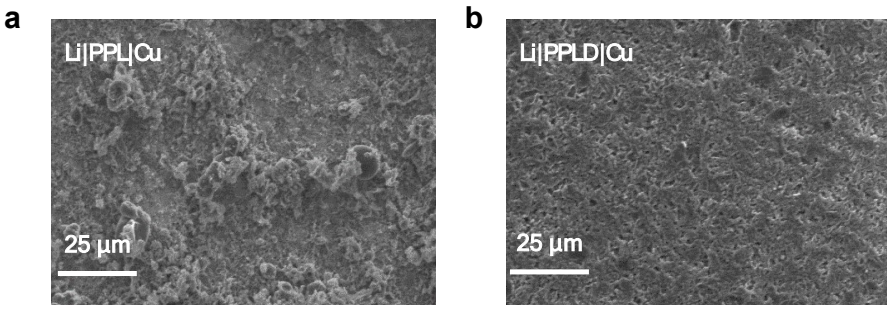

Figure S9. SEM images of Li metal deposits on Cu electrodes with (a) PPL and (b) PPLD separators after 50 cycles at a current density of 1.0 mA cm^{-2} and a capacity of 1.0 mAh cm^{-2}.

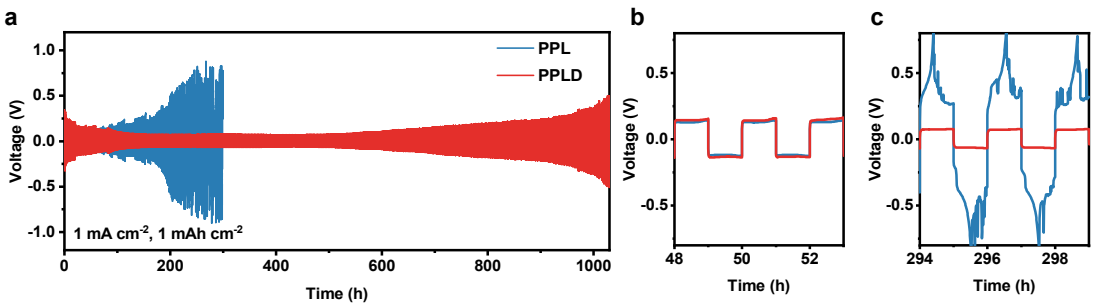

Figure S10. (a) Voltage–time curves and (b-c) magnified voltage–time curves of Li||Li symmetric cells with PPL and PPLD separators at a current density of 1.0 mA cm^{-2} and a capacity of 1.0 mAh cm^{-2}.

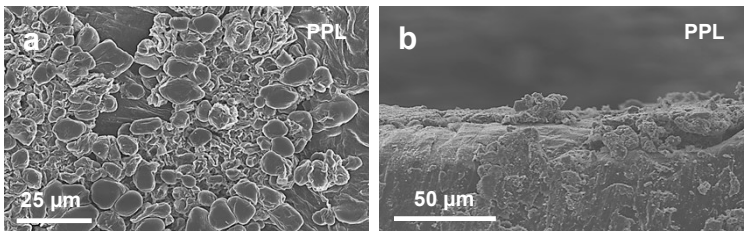

Figure S11. (a) Top-view and (b) cross-sectional SEM images for symmetrical Li||Li cells with PPL at current densities of 1 mA cm^{-2}, with an areal capacity of 1 mAh cm^{-2}.

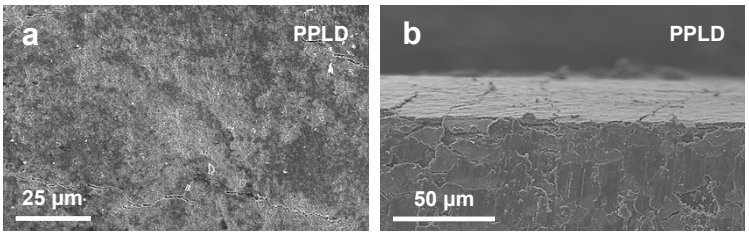

Figure S12. (a) Top-view and (b) cross-sectional SEM images for symmetrical Li||Li cells with PPLD at current densities of 1 mA cm^{-2}, with an areal capacity of 1 mAh cm^{-2}.

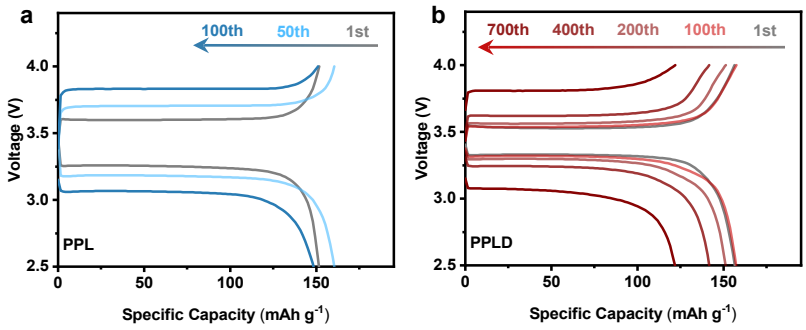

Figure S13. The capacity–voltage curves of the Li||LFP full cells with (a) PPL and (b) PPLD separators at 1 C.

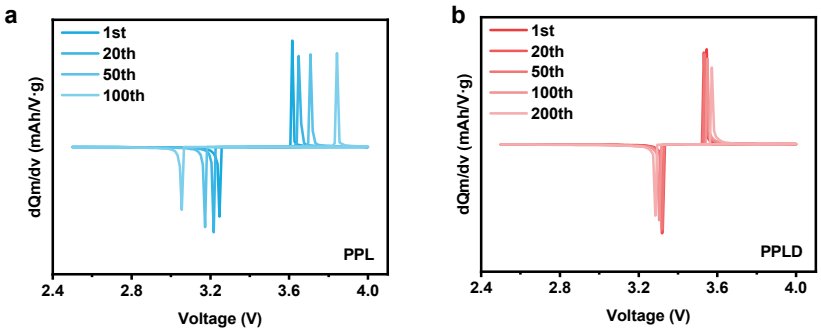

Figure S14. The dQ_m/dv curves of the Li||LFP full cells with (a) PPL and (b) PPLD separators at 1 C.

Table S3. Comparison to other reported work in terms of cathode areal capacity and long cycle life, corresponding to Figure 4d.

No.	Cathode areal capacity (mAh cm^{-2})	Battery performance		Data source
		Cycle number	Capacity retention	
1	1.1	150	93.4%	*Adv. Mater*. 2024, 36, 2406359
2	0.255	300	88.3%	*Energy Environ. Sci.*, 2024, 17, 4622–4633
3	1.68	200	86%	*Adv. Funct. Mater*. 2023, 33, 2305284
4	0.425	500	88%	*Adv. Funct. Mater*. 2025, 2505390
5	0.64	320	85.5%	*Adv. Sci.* 2022, 9, 2103930
6	3	400	90%	*Angew. Chem. Int. Ed.* 2023, 62, 202300771
7	0.68	500	80.3%	*Angew. Chem. Int. Ed.* 2023, 135, e202217458
8	2.04	300	N/A	*Adv. Mater.* 2021, 33, 2008133
9	2.2	200	92.2%	*Adv. Mater*. 2021, 33, 2006247
10	1.7	200	N/A	*Angew. Chem. Int. Ed.* 2023, 62, e202305723
11	1.87	360	95.7%	*Angew. Chem. Int. Ed.* 2025, 64, e202420973
12	1.02	600	N/A	*Adv. Sci.* 2022, 9, 2200411
13	0.868	600	N/A	*Adv. Funct. Mater.* 2021, 31, 2007255
14	1.275	700	80.26%	**This work**
15	2.72	500	85.04%	**This work**

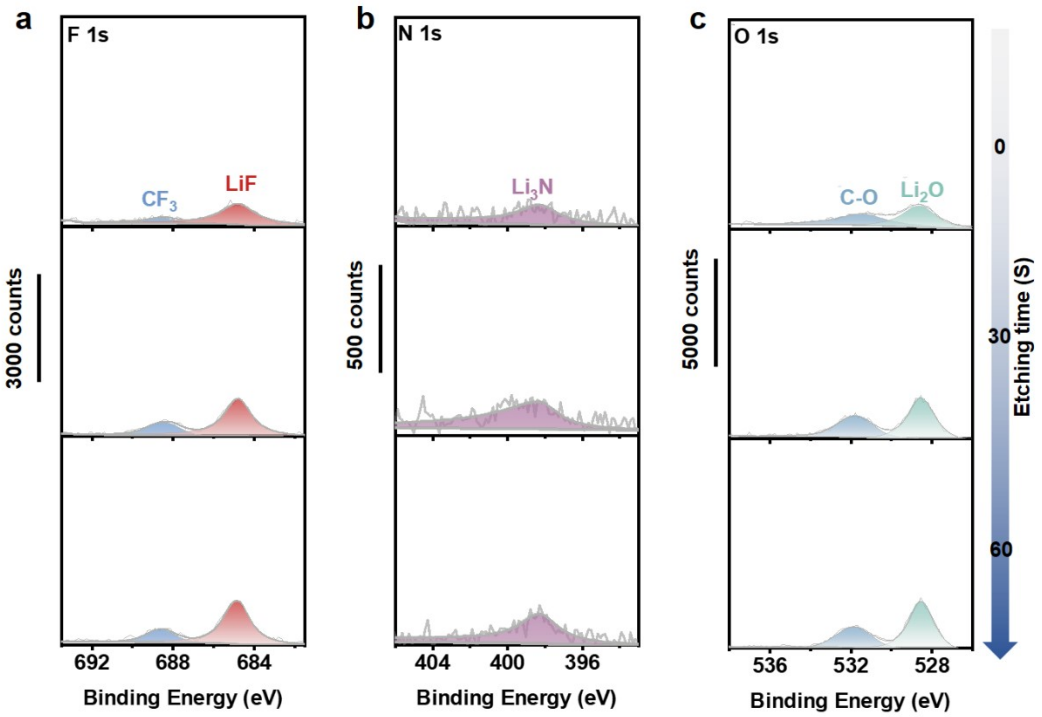

Figure S15. Detailed (a) F 1s, (b) N 1s, and (c) O 1s XPS spectra of the lithium surface after 50 cycles in Li||LFP full cells with PPL separator at different etching times.

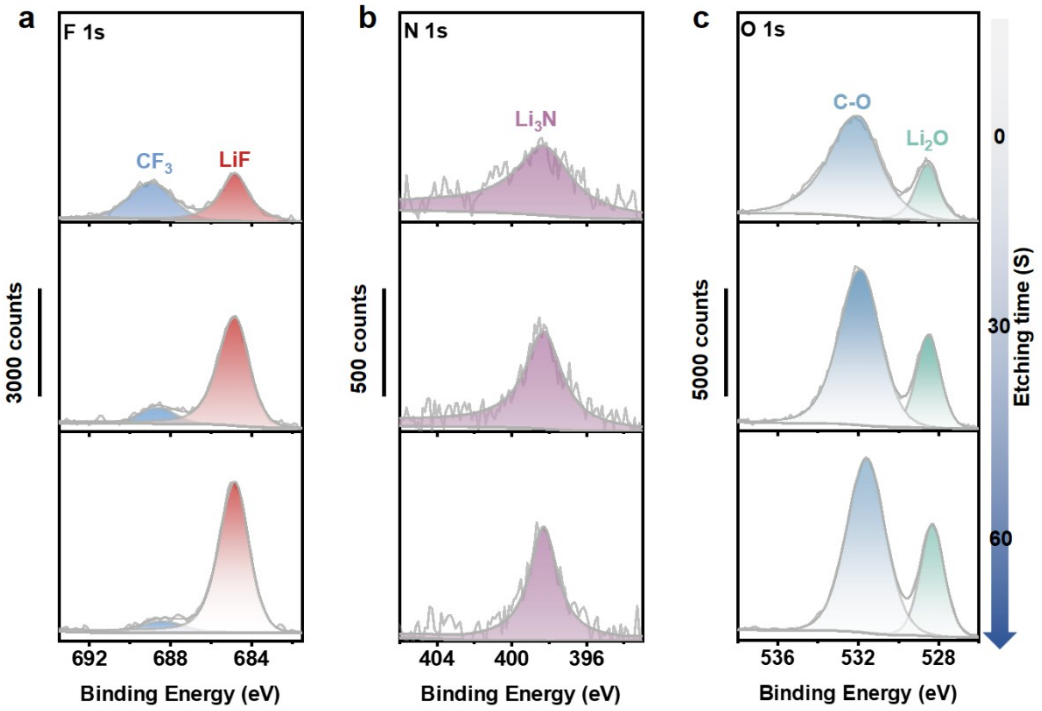

Figure S16. Detailed (a) F 1s, (b) N 1s, and (c) O 1s XPS spectra of the lithium surface after 50 cycles in Li||LFP full cells with PPLD separator at different etching times.

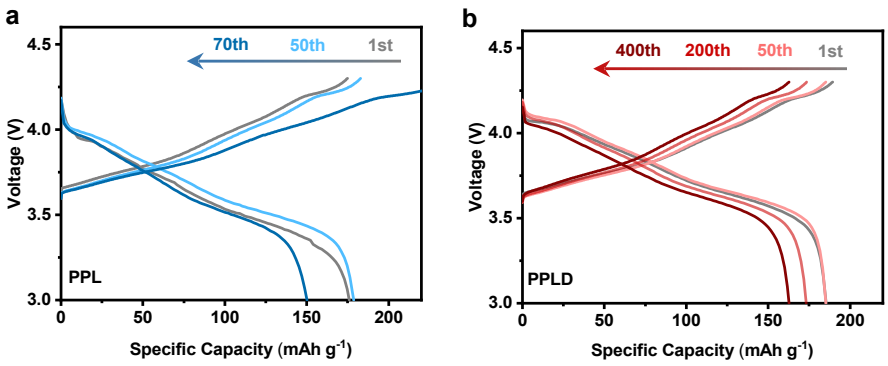

Figure S17. The capacity–voltage profiles of Li||NMC811 full cells with (a) PPL and (b) PPLD separators at 1 C.

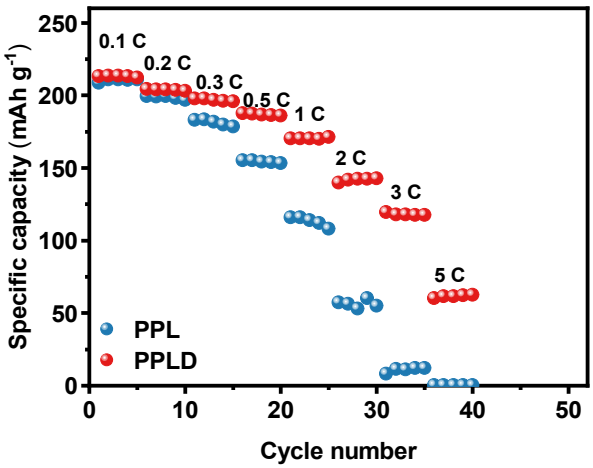

Figure S18. Rate performances of Li||NMC811 cells with PPL and PPLD separators from 0.1 to 5 C, respectively.

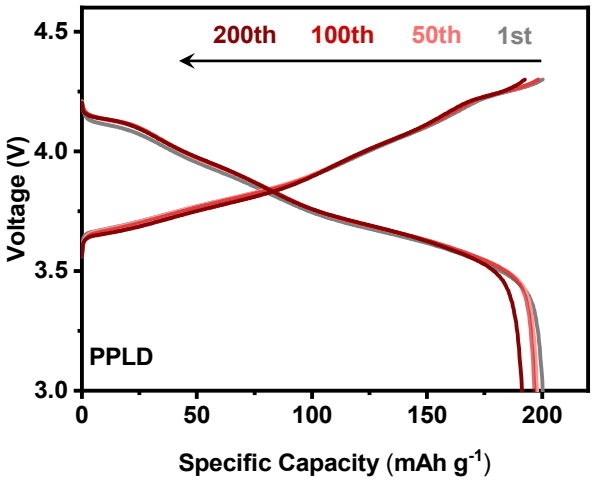

Figure S19. The voltage profiles of the Li||N MC811 pouch cell with the PPLD separator at 0.2 C.